Inorg. Chem. **2008**, *47*, 8562−8570

Forum

A-Site-Ordered Perovskites with Intriguing Physical Properties

Yuichi Shimakawa*

Institute for Chemical Research, Kyoto University, Uji, Kyoto 611-0011, Japan

Received April 18, 2008

Recent findings on intriguing physical properties of new A-site-ordered perovskite structure oxides are reviewed. High-pressure and high-temperature conditions stabilize the square-coordinated Jahn−Teller Cu^{2+} ions in the original 12-fold-coordinated positions of the perovskite structure. The special-ordered arrangement of the square-coordinated $A'O_4$ units that align perpendicularly to each other sets a characteristic structural framework, and the presence of Cu^{2+} ions at the A′ site and A′−B interactions play crucial roles for the diverse and intriguing physical properties.

1. Introduction

Oxides with perovskite or perovskite-related structures display a large variety of intriguing physical properties and raise lots of important fundamental issues in solid-state chemistry and physics. The researches of these materials are also of great interest because of their promising technological applications. For example, simple perovskite oxides such as $SrTiO_3$ and $BaTiO_3$ have been studied extensively and are already widely used in electronic devices. Some of the intriguing physical properties found recently in perovskite oxides and perovskite-related oxides are the high-T_C superconductivity of cupric oxides, the colossal magnetoresistance (MR) of manganese oxides, and the multiferroicity of $BiFeO_3$. These properties will be useful for functions in future electronics and spintronics.

The general formula of the perovskite oxide structure is ABO_3, in which A represents relatively large cations such as alkaline metal, alkaline-earth metal, and lanthanide ions and B generally represents transition-metal ions. The structure is described as a framework of corner-sharing BO_6 octahedra that contains A cations in 12-fold-coordinated sites. By the introduction of additional elements into the A or B site, ordered superstructures are often stabilized, and the special-ordered arrangements of the A or B cations in the perovskite structures open up possibilities for making compounds with new properties. Large numbers of B-site-ordered compounds have been obtained, and there are good review articles on them.[1,2] This paper therefore focuses on the A-site-ordered perovskites.

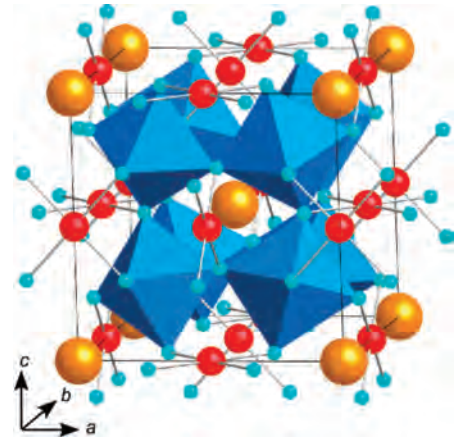

Figure 1. Crystal structure of $AA'_3B_4O_{12}$. The A ion (large sphere) and A′ ion (middle sphere) are ordered at the A site at a ratio of 1:3, and the B-site ions form BO_6 octahedra in a cubic ABO_3 perovskite structure.

A very unusual-ordered arrangement of the A-site ions produces $AA'_3B_4O_{12}$ complex perovskites, in which the A and A′ ions at the A site in the ABO_3 perovskite are ordered as shown in Figure 1. The A site accommodates alkaline metals, alkaline-earth metals, and lanthanides like those in simple perovskites. At the originally 12-fold-coordinated A′

* E-mail: shimak@scl.kyoto-u.ac.jp.

(1) Anderson, M. T.; Greenwood, K. B.; Taylor, G. A.; Poeppelmeir, K. R. *Prog. Solid State Chem.* **1993**, *102*, 375.
(2) Howard, C. J.; Kennedy, B. J.; Woodward, P. M. *Acta Crystallogr., Sect. B: Struct. Sci.* **2003**, *B59*, 463.

10.1021/ic800696u CCC: $40.75
Published on Web 09/29/2008

site, Jahn−Teller distorted ions such as Cu^{2+} and Mn^{3+} form square-coordinated units that align perpendicularly to each other. This special alignment of the $A'O_4$ squares and the significant tilting of the corner-sharing BO_6 octahedra make the $2a \times 2a \times 2a$ unit cell from the simple cubic perovskite structure. The presence of Cu^{2+} and/or Mn^{3+} transition-metal ions at the A′ site and the A′−B interactions play crucial roles for the diverse and intriguing physical properties of the materials with this characteristic structure.

Compounds with this structure were reported in pioneering works in the 1960−1970s.[3–6] The discovery of the temperature-independent colossal dielectric constant of $CaCu_3Ti_4O_{12}$ ($\sim 10^5$) accelerated research on this structure compound,[7–9] though recent careful studies by impedance analysis have revealed that this ceramic consists of semiconducting grains with insulating grain boundaries and that its large dielectric constant is due to the internal barrier layer capacitance.[10,11] Magnetic and transport properties of $CaCu_3Ru_4O_{12}$ have recently attracted attention because of their heavy-fermion-like behavior.[12] $NaMn_3Mn_4O_{12}$ is an A-site-ordered perovskite containing Jahn−Teller Mn^{3+}, and it shows a sequence of phase transitions associated with the ordering of the spin, charge, and orbital subsystems.[13]

We recently found several new A-site-ordered perovskite structure oxides with intriguing physical properties. In this paper, recent progresses of research on the new A-site-ordered perovskites are highlighted.

2. Experimental Section: High-Pressure Synthesis

Powder samples were prepared by solid-state reaction processes. $AA'_3B_4O_{12}$ compounds are often synthesized under high-pressure and high-temperature conditions in order to stabilize the square-coordinated Jahn−Teller ions in the original 12-fold-coordinated positions of the perovskite structure.

A cubic anvil-type high-pressure apparatus shown in Figure 2 was used for sample preparation.[14] The anvils are made of a superhard sintered tungsten carbide alloy. The six anvils synchronously compress the sample up to 10 GPa three-dimensionally through a pyrophyllite medium. Pressures up to 15 GPa were produced by using the "6−8" split device, which is a cascade type of multianvil apparatus.

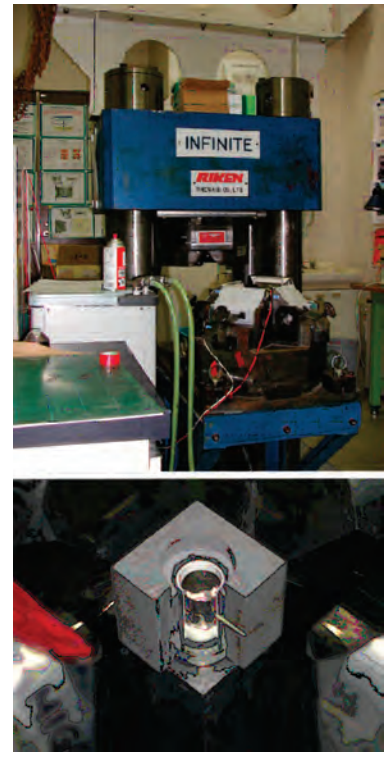

Figure 2. Schematic pictures of a cubic anvil-type high-pressure apparatus.

Appropriate mixtures of the starting raw materials, usually oxides and metals, were first pressed into pellets and calcined in air at 1000 °C. The calcined pellets were reground, packed into gold capsules with an oxidizing agent $KClO_4$, and then treated with high-pressure and high-temperature conditions. Typical conditions are 6−15 GPa and 800−1300 °C for 30 min followed by quenching.

3. Results and Discussion

3.1. $CaCu_3Ge_4O_{12}$−$CaCu_3Ti_4O_{12}$−$CaCu_3Sn_4O_{12}$. $CaCu_3Ge_4O_{12}$ and $CaCu_3Sn_4O_{12}$ were synthesized at 6 GPa and 1000 °C,[15,16] while $CaCu_3Ti_4O_{12}$ was prepared at 1000 °C for 20 h in ambient air.[7–9,17] All three samples crystallize the A-site-ordered cubic perovskite with $Im\bar{3}$ symmetry. Crystal structures of the compounds were analyzed with the Rietveld method from the synchrotron powder X-ray diffraction patterns. Although it is difficult to precisely refine the occupation factors for oxygen from the X-ray diffraction data, we see no anomaly in the occupation factors for all sites, suggesting the stoichiometric compositions for the three compounds. The refined structural parameters of the three compounds are summarized in Table 1.

In this series of compounds, the B site contains nonmagnetic ions, and only Cu^{2+} ($S = {}^1/_2$) spins at the A′ site contribute the

(3) Deschanvres, A.; Raveau, B.; Tollemer, F. *Bull. Soc. Chim. Fr.* **1967**, 4077.
(4) Marezio, M.; Dernier, P. D.; Chenavas, J.; Joubert, J. C. *J. Solid State Chem.* **1973**, *6*, 16.
(5) Bouchu, B.; Buevoz, J. L.; Chenavas, J.; Marezio, M. *Solid State Commun.* **1974**, *11*, 88.
(6) Chenavas, J.; Joubert, J. C.; Marezio, M.; Bochu, B. *J. Solid State Chem.* **1975**, *14*, 25.
(7) Subramanian, M. A.; Li, D.; Duan, N.; Reisner, B. A.; Sleight, A. W. *J. Solid State Chem.* **2000**, *151*, 323.
(8) Ramirez, A. P.; Subramanian, M. A.; Gardel, M.; Blumberg, G.; Li, D.; Vogt, T.; Shapiro, S. M. *Solid State Commun.* **2000**, *115*, 217.
(9) Homes, C. C.; Vogt, T.; Shapiro, S. M.; Wakimoto, S.; Ramirez, A. P. *Science* **2001**, *293*, 673.
(10) Sinclair, D. C.; Adams, T. B.; Morrison, F. D.; West, A. R. *Appl. Phys. Lett.* **2002**, *80*, 2153.
(11) Adams, T. B.; Sinclair, D. C.; West, A. R. *Adv. Mater.* **2002**, *14*, 1321.
(12) Kobayashi, W.; Terasaki, I.; Takeya, J.; Tsukada, I.; Ando, Y. *J. Phys. Soc. Jpn.* **2004**, *73*, 2373.
(13) Prodi, A.; Gilioli, E.; Gauzzi, A.; Licci, F.; Marezio, M.; Bolzoni, F.; Huang, Q.; Santoro, A.; Lin, J. W. *Nat. Mater.* **2004**, *3*, 48.
(14) Takano, M.; Takeda, Y.; Ohtaka, O. In *Encyclopedia of Inorganic Chemistry*; King R. B., ed.; Vol. *3*, p 1372; John Wiley & Sons: Chichester, 1994.
(15) Shiraki, H.; Saito, T.; Yamada, T.; Tsujimoto, M.; Azuma, M.; Kurata, H.; Isoda, S.; Takano, M.; Shimakawa, Y. *Phys. Rev. B* **2007**, *76*, 140403(R)
(16) Ozaki, Y.; Ghedira, M.; Chenavas, J.; Joubert, J. C.; Marezio, M. *Acta Crystallogr., Sect. B: Struct. Crystallogr. Cryst. Chem.* **1977**, *B33*, 3615.
(17) Bochu, B.; Deschizeaux, M. N.; Joubert, J. C.; Collomb, A.; Chenavas, J.; Marezio, M. *J. Solid State Chem.* **1979**, *29*, 291.

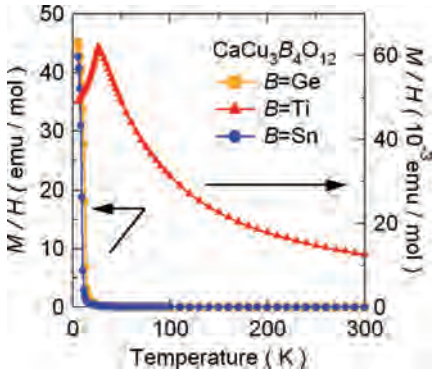

Figure 3. Temperature dependence of the magnetic susceptibility of $CaCu_3B_4O_{12}$ (B = Ge, Ti, Sn) measured in an external magnetic field of 1000 Oe.

Table 1. Structural and Magnetic Parameters of $CaCu_3Ge_4O_{12}$, $CaCu_3Ti_4O_{12}$, and $CaCu_3Sn_4O_{12}$

	$CaCu_3Ge_4O_{12}$	$CaCu_3Ti_4O_{12}$	$CaCu_3Sn_4O_{12}$
radius (B) (Å)	0.530	0.605	0.690
a (Å)	7.26702(1)	7.39142(1)	7.64240(8)
Cu−O−Cu (deg)	100.67(4)	100.76(3)	100.67(9)
Cu−Cu (Å)	3.6335(1)	3.6957(1)	3.8212(1)
Cu−O (Å)	1.9818(10)	1.9710(9)	1.9868(20)
magnetism	FM	AFM	FM
T_C or T_N (K)	13	25	10
θ_{CW} (K)	16.4	−32.6	12.3
C_{CW} (emu K/mol)	1.158	1.365	1.224
μ_{eff} (μ_B/Cu)	1.76	1.91	1.81

magnetic properties. Figure 3 shows the temperature dependence of the magnetic susceptibility of each compound measured with a superconducting quantum interference device (SQUID) magnetometer under an external magnetic field of 1 kOe. Sharp increases in magnetization at 13 and 10 K for $CaCu_3Ge_4O_{12}$ and $CaCu_3Sn_4O_{12}$, respectively, indicate ferromagnetic transitions at these temperatures. For $CaCu_3Ti_4O_{12}$, in contrast, a sharp peak due to the antiferromagnetic transition is observed at 25 K.[8,18,19] Magnetic susceptibility above the transition temperature obeys the Curie−Weiss law, $M/H = (C_{CW} - \theta_{CW})/T$, and the Weiss temperature θ_{CW} and the Curie constant C_{CW} of each compound are also summarized in Table 1. Effective magnetic moments, μ_{eff}, calculated from the Curie constants by using $g = 2.00$ strongly suggest the presence of Cu^{2+} ($S = {}^1/_2$; $\mu_{eff} = 1.73$) localized spins. As shown in Figure 4, saturation magnetizations at 5 K and 10 kOe are 0.94 and 0.98 μ_B/Cu for $CaCu_3Ge_4O_{12}$ and $CaCu_3Sn_4O_{12}$, respectively, which also supports the ferromagnetic alignment of Cu^{2+} ($S = {}^1/_2$) spins.

It is interesting that the A-site Cu^{2+} spins can align either ferromagnetically or antiferromagnetically within the same structural framework, depending on the nonmagnetic B-site ion. The relationships between structural features and magnetic properties are worth noting. As the size of the B-site ion[20] increases from Ge to Sn, the lattice constant and the Cu−Cu bond distance increase from $CaCu_3Ge_4O_{12}$ to $CaCu_3Sn_4O_{12}$. The Cu−O distance and Cu−O−Cu bond angle, in contrast, are almost constant among these compounds. As for the magnetic properties, $CaCu_3Ge_4O_{12}$ and $CaCu_3Sn_4O_{12}$, with the shortest and longest Cu−Cu bond distances, respectively, show ferromagnetic behavior, whereas $CaCu_3Ti_4O_{12}$, with the intermediate Cu−Cu bond distance, exhibits antiferromagnetic properties. Therefore, simple magnetic interactions between the Cu^{2+} spins cannot explain the behavior.

(18) Koitzsch, A.; Blumberg, G.; Gozar, A.; Dennis, B.; Ramirez, A. P.; Trebst, S.; Wakimoto, S. *Phys. Rev. B* **2002**, *65*, 52406.
(19) Kim, Y. J.; Wakimoto, S.; Shapiro, S. M.; Gehring, P. M.; Ramirez, A. P. *Solid State Commun.* **2002**, *121*, 625.
(20) Shannon, R. D. *Acta Crystallogr., Sect. A* **1976**, *32*, 751.

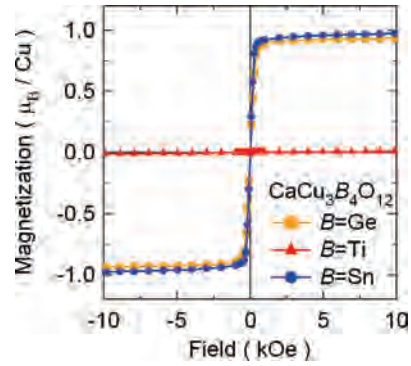

Figure 4. Magnetization of $CaCu_3B_4O_{12}$ (B = Ge, Ti, Sn).

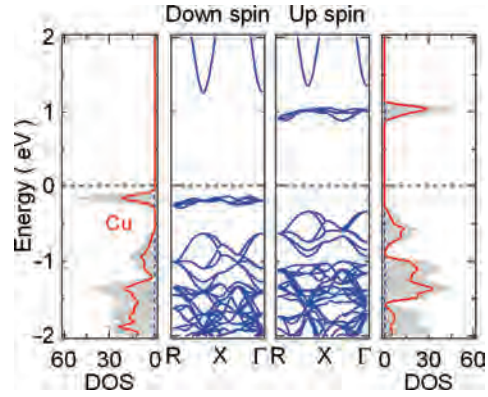

Figure 5. Calculated DOSs (states/eV cell spin) and band structure for ferromagnetic $CaCu_3Ge_4O_{12}$. Total DOSs (shaded region) and partial DOSs of Cu (solid line) and Ge (dashed line) are shown in the figures.

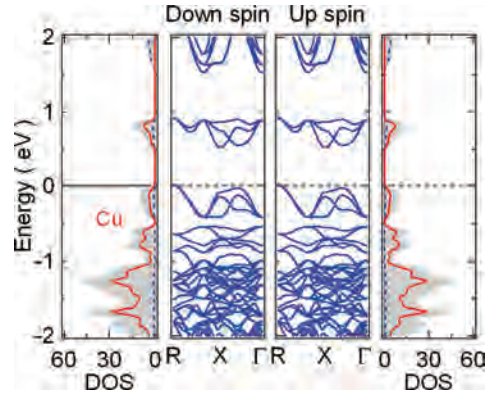

Figure 6. Same as that for Figure 5 but for antiferromagnetic $CaCu_3Ti_4O_{12}$.

The electronic structures were then investigated for $CaCu_3Ge_4O_{12}$, $CaCu_3Ti_4O_{12}$, and $CaCu_3Sn_4O_{12}$ by full potential linearized augmented plane-wave (FLAPW) first-principle calculations within the generalized gradient approximation exchange-correlation function. The lattice parameters and the atomic positional parameters obtained experimentally from the structural analysis were used for the calculations. For the spin-polarized states, electronic structures for ferromagnetic and antiferromagnetic arrangements of Cu^{2+} spins were calculated with a $Pm\bar{3}$ structure model, which is confirmed by a neutron diffraction measurement on $CaCu_3Ti_4O_{12}$.[19,21] In this antiferromagnetic arrangement, the Cu^{2+} spins are ordered along the [111] direction. The calculations confirmed that the ferromagnetic states are stable compared to the antiferromagnetic states for $CaCu_3Ge_4O_{12}$ and $CaCu_3Sn_4O_{12}$ by 12.5 and 7.1 meV, respectively.

(21) Lacroix, C. *J. Phys. C* **1980**, *13*, 5125.

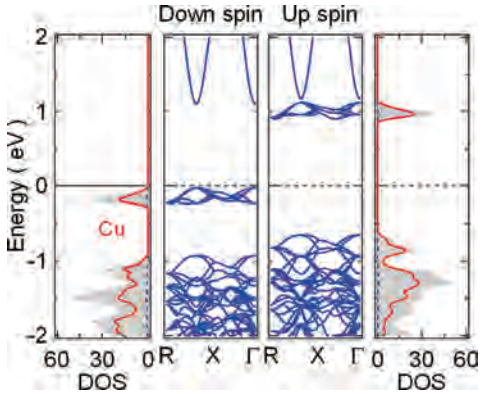

Figure 7. Same as that for Figure 5 but for ferromagnetic $CaCu_3Sn_4O_{12}$.

In contrast, the antiferromagnetic state is energetically lower than the ferromagnetic state by 82.0 meV for $CaCu_3Ti_4O_{12}$, essentially the same as that reported previously.[22,23] The results obtained from the calculations are consistent with the observed experimental results of magnetic properties.

Figures 5–7 respectively show the density of states (DOSs) and the band structures near the Fermi level for the three compounds. When the DOSs of the three compounds are compared, the widths of the bands located just below the Fermi level E_F, which mainly consisting of Cu 3d and O 2p orbitals, show a significant difference between the ferromagnetic and antiferromagnetic compounds. The corresponding bands are narrow (~0.3 eV) for the ferromagnetic $CaCu_3Ge_4O_{12}$ and $CaCu_3Sn_4O_{12}$. For $CaCu_3Ti_4O_{12}$, in contrast, the bands are rather broad (~0.5 eV), suggesting the significant hybridization of orbitals. Because the empty Ti 3d band can hybridize with the O 2p and Cu 3d orbitals near E_F, contribution of the Ti 3d band should lead to the broad-band structure.

In the $CaCu_3B_4O_{12}$ crystal structure, the CuO_4 squares with Jahn−Teller Cu^{2+} ions align perpendicularly to each other. This special alignment of the CuO_4 squares provides direct-exchange interaction between the nearest Cu^{2+} spins but does not induce normal superexchange interaction through O ions. Such a direct-exchange interaction gives rise to ferromagnetic behavior in $CaCu_3Ge_4O_{12}$ and $CaCu_3Sn_4O_{12}$. This may also explain why the ferromagnetic T_C (13 K) for $CaCu_3Ge_4O_{12}$ with the shorter Cu−Cu distance is slightly higher than that (10 K) for $CaCu_3Sn_4O_{12}$ with the longer one. In $CaCu_3Ti_4O_{12}$, in contrast, involvement of Ti 3d orbitals produces the antiferromagnetic superexchange interaction between the Cu^{2+} spins,[21] which overcomes the ferromagnetic direct interaction.

Because the ferromagnetic and antiferromagnetic interactions between the Cu^{2+} ($S = {}^1/_2$) spins at the A′ site are competing, magnetic behaviors in $CaCu_3(Ge_{1-x}Ti_x)_4O_{12}$ and $CaCu_3(Ti_{1-y}Sn_y)_4O_{12}$ solid solutions are especially interesting.[24] Shown in Figures 8 and 9 are temperature dependences of the magnetic susceptibility and inverse susceptibility. The magnetic properties in the solid solutions change gradually and systematically. Above the transition temperature, the susceptibility obeys the Curie−Weiss law, and the Curie constant C_{CW} and Weiss temperature θ_{CW} of each solid solution compound are shown in Figure 10. Note that the Curie constant for each compound is ~1.13 emu K/mol, which gives an effective magnetic moment of 1.73 μ_B by using $g = 2.00$, suggesting that there are Cu^{2+} ($S = {}^1/_2$) localized spins.

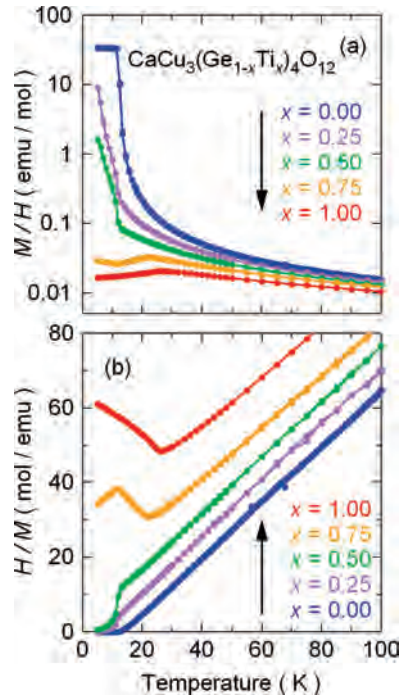

Figure 8. Temperature dependence of (a) the magnetic susceptibility and (b) the inverse susceptibility for $CaCu_3(Ge_{1-x}Ti_x)_4O_{12}$.

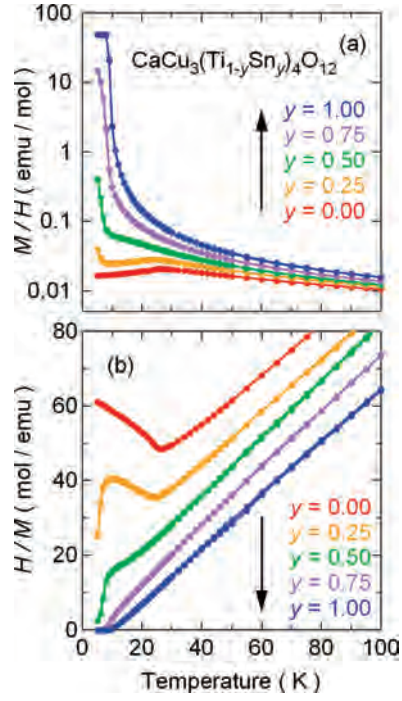

Figure 9. Same as that for Figure 8 but for $CaCu_3(Ti_{1-y}Sn_y)_4O_{12}$.

What is of particular interest here is that the Weiss temperature changes from positive to negative as the material changes from $CaCu_3Ge_4O_{12}$ to $CaCu_3Ti_4O_{12}$ and then changes back to a positive value as the material changes from $CaCu_3Ti_4O_{12}$ to $CaCu_3Sn_4O_{12}$. This implies that the effective magnetic interaction between Cu^{2+} spins changes gradually from ferromagnetic to antiferromagnetic to ferromagnetic in the solid solution. More important, the Weiss temperature crosses zero at intermediate compositions $x \sim 0.4$ and $y \sim 0.6$. The change in the Cu−Cu distance, also plotted in Figure 10, is worth noting. As the magnetic property changes from ferromagnetic to antiferromagnetic to ferromagnetic, the Cu−Cu

(22) He, L.; Neaton, J. B.; Cohen, M. H.; Vanderbilt, D.; Homes, C. C. *Phys. Rev. B* **2002**, *65*, 214112.
(23) Li, G.-L.; Yin, Z.; Zhang, M.-S. *Phys. Lett. A* **2005**, *344*, 238.
(24) Shimakawa, Y.; Shiraki, H.; Saito, T. 2008, submitted for publication.

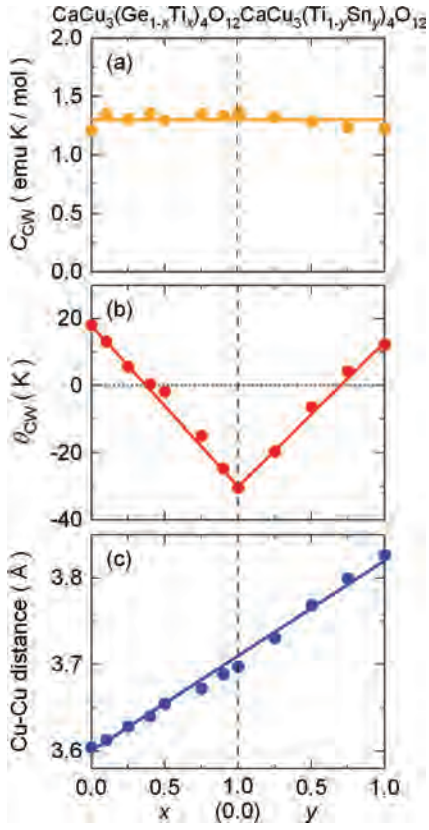

Figure 10. Changes in (a) the Curie constant C_{CW}, (b) the Weiss temperature θ_{CW}, and (c) the Cu−Cu distance as a function of x in $CaCu_3(Ge_{1-x}Ti_x)_4O_{12}$ and y in $CaCu_3(Ti_{1-y}Sn_y)_4O_{12}$.

distance increases monotonically. In the solid solution, the ferromagnetic direct-exchange and antiferromagnetic superexchange interactions are competing. At the critical compositions for which the Weiss temperature is 0 K, the Cu−Cu ferromagnetic direct exchange and the Cu−O−Ti−O−Cu antiferromagnetic superexchange interactions are perfectly balanced.

The ferromagnetic-to-antiferromagnetic-to-ferromagnetic transitions in the present system are in sharp contrast to the switching from ferromagnetism to antiferromagnetim reported to occur in the $SeCuO_3$−$TeCuO_3$ perovskite[25,26] and Ca_2CrSbO_6−Sr_2CrSbO_6 double-perovskite[27] systems, in both of which the superexchange bond angles for the B-site cations determine the magnetic interactions. In the $SeCuO_3$−$TeCuO_3$ perovskite system, negative chemical pressure due to the substitution of the Te ion for the A-site Se causes a change in a highly distorted Cu−O−Cu bond angle. The 90° ferromagnetic superexchange interaction switches to the 180° antiferromagnetic one at the crossover angle 127°. In the Ca_2CrSbO_6−Sr_2CrSbO_6 double-perovskite system, rock-salt-type ordering of the B-site cations produces frustrated antiferromagnetism through Cr−O−Sb−O−Cr superexchange interaction. The ferromagnetism arises with the significant tilting of the BO_6 octahedra with a large bend of the superexchange path. These behaviors in magnetism with respect to the superexchange bond angle are well understood with Kanamori−Goodenough's rule. Thus, the difference from the bond-angle mechanism makes the present system unique.

(25) Subramanian, M. A.; Ramirez, A. P.; Marshall, W. J. *Phys. Rev. Lett.* **1999**, *82*, 1558.
(26) Lawes, G.; Ramirez, A. P.; Varma, C. M.; Subramanian, M. A. *Phys. Rev. Lett.* **2003**, *91*, 257208.
(27) Retuerto, M.; Garcia-Hernandez, M.; Martinez-Lope, M. J.; Fernandez-diaz, M. T.; Attfield, J. P.; Alonso, J. A. *J. Mater. Chem.* **2007**, *17*, 3555.

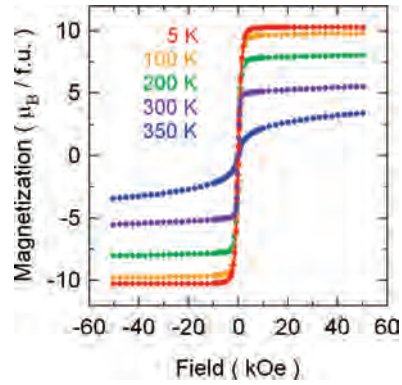

Figure 11. Magnetization-field curves of $BiCu_3Mn_4O_{12}$ at various temperatures.

The present solid solutions provide a model system for the study of magnetism; i.e., the simple $S = {}^1/_2$ cubic spin sublattice sets the stages of both ferromagnetism and antiferromagnetism. The cubic $Im\bar{3}$ structure in $CaCu_3(Ge,Ti,Sn)_4O_{12}$ is intact throughout the entire range of solid solution composition, in contrast to the orthorhombic *Pnma* and monoclinic $P2_1/n$ space groups for $(Se,Te)CuO_3$ and $(Ca,Sr)_2CrSbO_6$, respectively. Either ferromagnetism or antiferromagnetim arises within the same simple structural framework.

3.2. $CaCu_3Mn_4O_{12}$−$LaCu_3Mn_4O_{12}$−$BiCu_3Mn_4O_{12}$. Introducing magnetic ions into the B site causes the A′-site Cu^{2+} spins to couple with the B-site spins antiferromagnetically, leading to a ferrimagnetic state. In the ferrimagnetic insulator $CaCu_3Mn_4O_{12}$,[6] the large ferrimagnetic moment of 9 μ_B/f.u. below the ferrimagnetic transition temperature (355 K) is due to antiparallel alignment of the A′-site Cu^{2+} ($S = {}^1/_2$) and the B-site Mn^{4+} ($S = {}^3/_2$) spins. The material is a semiconductor with a small spin-asymmetric gap, and thermally induced electrons doped into up-spin Mn e_g levels give rise to spin-polarized intergrain low-field MR.[28,29]

Substituting trivalent La or Bi ions for the divalent Ca ions produces a half-metallic nature with spin-polarized conduction carriers.[30−32] Here, the details of $BiCu_3Mn_4O_{12}$ are described. The sample was prepared under 6 GPa and 1000 °C conditions. In a simple ionic picture, substitution of Bi^{3+} for Ca^{2+} produces a mixed valence of $Mn^{3.75+}$ in the nominal composition. A bond valence sum (BVS) calculation[33] from the refined structural parameters gives 3.73+ for the B-site Mn ion, which is close to the nominal valence of 3.75+.

$BiCu_3Mn_4O_{12}$ shows spontaneous magnetization below 350 K. The field and temperature dependences of magnetization are shown in Figures 11 and 12, respectively. The observed saturation magnetization at 5 K is about 10.5 μ_B/f.u., which is quite close to the value expected from an antiparallel alignment between Mn and Cu spins for the composition of $BiCu_3Mn^{3+}Mn^{4+}{}_3O_{12}$ (Cu^{2+}, $S = {}^1/_2$; Mn^{3+}, $S = 2$; Mn^{4+}, $S = {}^3/_2$).

The resistivity of $BiCu_3Mn_4O_{12}$ is as low as 10^3 Ω cm, and the material clearly shows low-field MR below the ferrimagnetic transition temperature. Figure 13 shows the MR ratio, defined as $MR(H) = [R(H) - R(0)]/R(0)$, under magnetic fields at various

(28) Zeng, Z.; Greenblatt, M.; Subramanian, M. A.; Croft, M. *Phys. Rev. Lett.* **1999**, *82*, 3164.
(29) Weht, R.; Pickett, W. E. *Phys. Rev. B* **2001**, *65*, 014415.
(30) Alonso, J. A.; Sanchez-Benitez, J.; de Andres, A.; Martinez-Lope, M. J.; Casais, M. T.; Martinez, J. L. *Appl. Phys. Lett.* **2003**, *83*, 2623.
(31) Liu, X.-J.; Xiang, H.-P.; Cai, P.; Hao, X.-F.; Wu, Z.-J.; Meng, J. *J. Mater. Chem.* **2006**, *16*, 4243.
(32) Takata, K.; Yamada, I.; Azuma, M.; Takano, M.; Shimakawa, Y. *Phys. Rev. B* **2007**, *76*, 024429.
(33) Brown, I. D.; Altermatt, D. *Acta Crystallogr., Sect. B: Struct. Sci.* **1985**, *41*, 244.

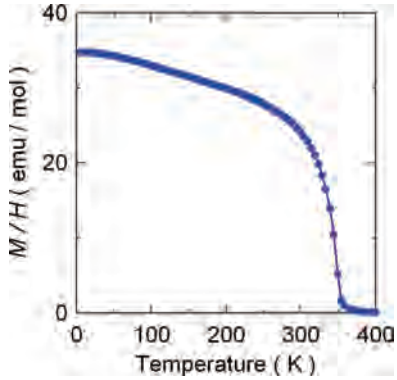

Figure 12. Temperature dependence of magnetization of $BiCu_3Mn_4O_{12}$.

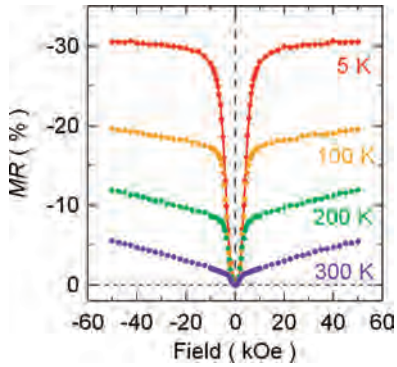

Figure 13. MR ratios of $BiCu_3Mn_4O_{12}$ at various temperatures.

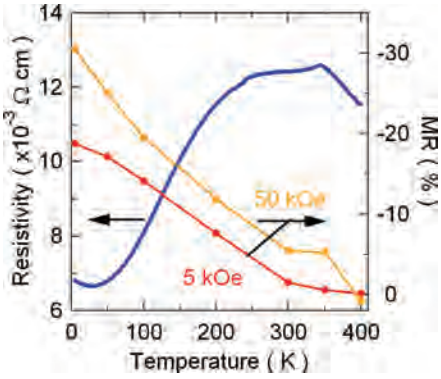

Figure 14. Temperature dependence of the resistivity at zero applied field and MR ratios at 5 and 50 kOe.

temperatures. At 5 K, the low-field MR below 10 kOe is as large as −28%, and MR reaches −31% at 50 kOe. The changes in MR are quite consistent with the changes in magnetization. At low applied fields of less than 10 kOe, the resistivity significantly decreases with increasing magnetization, and it saturates in accordance with the saturation in magnetization. Because the change in magnetization in a polycrystalline sample below T_C corresponds to the change in alignment of magnetic domains, the observed large MR under low magnetic field should be a result of a grain- or domain-boundary effect. It should also be noted that MR is still significant at room temperature. The observed MR values are about −2% and about −6% at 1 and 50 kOe, respectively.

The temperature dependence of the resistivity of $BiCu_3Mn_4O_{12}$ is illustrated in Figure 14. It is worth mentioning that the resistivity at $H = 0$ displays a metallic behavior below T_C and a semiconducting behavior above T_C. The distinct change in the temperature dependence of the resistivity at T_C implies that the transport properties of $BiCu_3Mn_4O_{12}$ are strongly affected by the magnetic properties. In the ferrimagnetic state below T_C, the sample changes

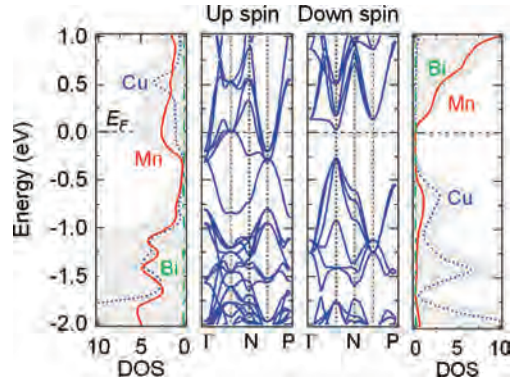

Figure 15. Calculated DOSs (states/eV cell spin) and band structure for the ferrimagnetically ordered ground state of $BiCu_3Mn_4O_{12}$. Total DOSs (shaded region) and partial DOSs of Cu (dashed line), Mn (solid line), and Bi (dashed−dotted line) are shown in the figures.

to a metallic state and the resistivity decreases. It should also be pointed out that the MR is observed over a wide temperature range below T_C, and the value increases with a decrease in the temperature. This is quite similar to that observed in Sr_2FeMoO_6,[34] in which low-field MR is attributed to the grain- or domain-boundary effect in polycrystalline samples.

The electronic structure of $BiCu_3Mn_4O_{12}$ was calculated for the ferrimagnetically ordered ground state as indicated by the magnetic measurement. The calculated total magnetic moment is 10.00 μ_B/f.u., which agrees well with the experimentally observed saturated magnetic moment and the moment expected from the ferrimagnetic ordering of Mn and Cu spins for the composition of $BiCu_3Mn^{3+}Mn^{4+}{}_3O_{12}$. The calculated band structures and the corresponding DOSs for up and down spins are shown in Figure 15. In sharp contrast to the spin-asymmetric insulating band structure of $CaCu_3Mn_4O_{12}$, up-spin conduction bands cross the Fermi level. These bands mainly consist of Mn e_g states. This is consistent with the ionic picture, in which the Bi^{3+} incorporation induces mixed valence for the Mn ion such as $Mn^{3.75+}$. It should be noted that the band structure for $BiCu_3Mn_4O_{12}$ is also spin asymmetric, and the half-metallic nature produces spin-polarized conduction electrons in this material. The down-spin bands at the valence band maximum, on the other hand, have a strong Cu 3d character hybridized with O 2p. The magnetic and transport properties and the calculated band structure of $BiCu_3Mn_4O_{12}$ are very similar to those reported for $LaCu_3Mn_4O_{12}$.[30,31] The bands originating from Bi ions thus appear to play a less important role in the metallic conductivity and MR.

3.3. $CaCu_3Fe_4O_{12}$. Another ferrimagnetic A-site-ordered perovskite is $CaCu_3Fe_4O_{12}$,[35] which is a new Fe^{4+}-containing oxide discovered three decades after the first one was.[36–38] High-pressure conditions above 9 GPa stabilize this unusually high ionic state. In the characterization process, we noticed that Fe^{3+} tended to substitute at the A′ site but the amount decreased as the applied pressure was raised. The sample was thus prepared at the highest available pressure of 15 GPa. The amount of Fe^{3+} at the A′ site is estimated at 3%.

(34) Kobayshi, K.-I.; Kimura, T.; Sawada, H.; Terakura, K.; Tokura, Y. *Nature* **1998**, *395*, 677.
(35) Yamada, I.; Takata, K.; Hayashi, N.; Shinohara, S.; Azuma, M.; Mori, S.; Muranaka, S.; Shimakawa, Y.; Takano, M. *Angew. Chem. Int. Ed.* **2008**, in press.
(36) Gallagher, P. K.; Buchanan, D. N.; Macchesney, J. B. *J. Chem. Phys.* **1964**, *41*, 2429.
(37) Kanamaru, F.; Miyamoto, H.; Mimura, Y.; Koizumi, M.; Shimada, M.; Kume, S.; Shin, S. *Mater. Res. Bull.* **1970**, *5*, 257.
(38) Takeda, Y.; Naka, S.; Takano, M.; Shinjo, T.; Takada, T.; Shimada, M. *Mater. Res. Bull.* **1978**, *13*, 61.

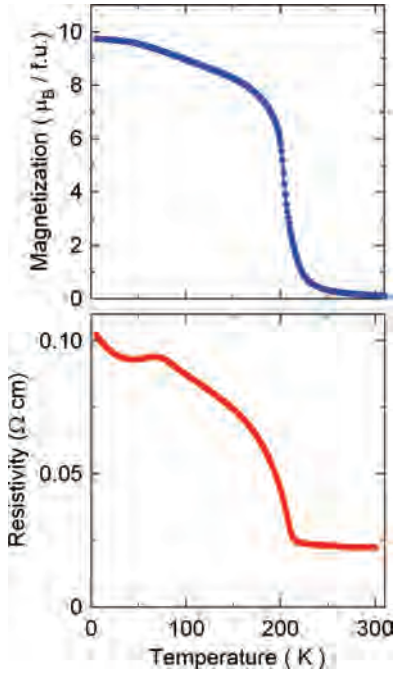

Figure 16. Temperature dependence of the resistivity and magnetization measured in an external magnetic field of 10 kOe for $CaCu_3Fe_4O_{12}$.

The resistivity of $CaCu_3Fe_4O_{12}$ is as low as $\sim 2 \times 10^{-2}$ Ω cm above 210 K but increases below this temperature, as shown in Figure 16. A spontaneous magnetization also appears below this temperature. The observed saturation magnetization of 9.7 μ_B/f.u. is close to the ferrimagnetic moment of 13 μ_B/f.u. expected from the ferrimagnetic ordering between Cu^{2+} ($S = {}^1/_2$) and Fe^{4+} ($S = 2$). The magnetization decreased as the amount of Fe^{3+} at the A′ site increased, but the transition temperature T_C did not change remarkably. It seemed that Fe^{3+} at the A′ site disturbed magnetism seriously but only in a limited region around the A′ site. In further detail, the resistivity tended to level off or even decrease at ~70 K, and the reason for this is not clear.

Microscopic details of the transition were studied using Mössbauer spectroscopy. The spectrum taken at 300 K shown in Figure 17 consists of three components superimposed at a ratio of 93:4:3. These components are (i) a singlet with an isomer shift (IS) of 0.15 mm/s relative to α-Fe, (ii) a quadrupole doublet with an IS of 0.38 mm/s and a quadrupole splitting ΔE of 1.83 mm/s, and (iii) a magnetic sextet due to an α-Fe_2O_3 impurity. The IS of component i for the major Fe^{4+} species at the B site is considerably larger than those of ~0.07 mm/s for $CaFeO_3$ and $SrFeO_3$,[36,39,40] indicating that their real electronic state is a little bit closer to Fe^{3+}. This interpretation is consistent with the charge transfer suggested from the BVS calculation, which gives rather unusual 2.43+ for Cu and 3.77+ for Fe. The second component having an Fe^{3+}-like IS is assigned to Fe^{3+} at the A′ site. The large quadrupole splitting most likely reflects the strong anisotropy of the square coordination. Such an Fe^{3+} species at the A′ site was observed also for a related oxide, $CaMn^{3+}{}_3Mn^{4+}{}_4O_{12}$, doped with ^{57}Fe as a Mössbauer spectroscopic probe.[41]

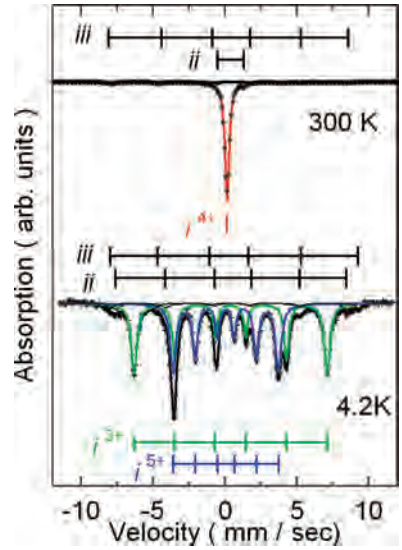

Figure 17. Mössbauer spectra taken at 300 and 4.2 K. The dots and the solid lines represent the observed spectra and the fittings, respectively. The components are assigned as follows: i^{4+}, Fe^{4+} occupying the B site; ii, Fe^{3+} partially applying at the A′ site; iii, an impurity, α-Fe_2O_3; i^{3+}, Fe^{3+} at the B site; i^{5+}, Fe^{5+} at the B site.

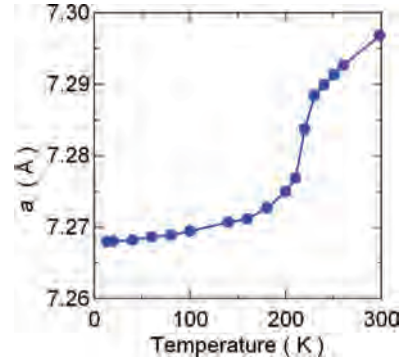

Figure 18. Temperature dependence of the cubic lattice constant a for $CaCu_3Fe_4O_{12}$.

The spectra below T_C are magnetically split. Furthermore, as can be seen clearly in the 4.2 K spectrum, the Fe^{4+} component at the B site is divided into two components having largely different hyperfine parameters but equal intensities, i^{3+} and i^{5+}, revealing the occurrence of charge disproportionation of the $CaFeO_3$ type. The ISs for Fe^{3+} (i^{3+}) and Fe^{5+} (i^{5+}) at 4.2 K are respectively 0.39 and 0.05 mm/s, and their magnetic hyperfine fields are respectively 417 and 227 kOe. Whether the 210 K transition is of first or second order is not clear, but the magnetic ordering, the charge disproportionation, and the resistivity change apparently set in concomitantly. Structural studies on the low-temperature phase using electron and synchrotron X-ray diffractions reveal the rock-salt-type ordering of Fe^{3+} and Fe^{5+} in the appearance of the (111) reflection most typically. The lattice symmetry is lowered to $Pn\bar{3}$, when the lattice constant suddenly decreases as shown in Figure 18. The low-temperature structure provides two kinds of B sites, 4b and 4c, arranged in the rock-salt manner. According to the structural analysis for the synchrotron X-ray diffraction data at 90 K, the Fe−O bonds are split into 1.970(3) Å for Fe^{3+} and 1.893(3) Å for Fe^{5+}, as is also found in $CaFeO_3$.[42,43] Now the aforementioned

(39) Takano, M.; Nakanishi, N.; Takeda, Y.; Naka, S.; Takada, T. *Mater. Res. Bull.* **1977**, *12*, 923.
(40) Kawasaki, S.; Takano, M.; Takeda, Y. *J. Solid State Chem.* **1996**, *121*, 174.
(41) Presniakov, I. A.; Rusakov, V. S.; Gubaidulina, T. V.; Sobolev, A. V.; Baranov, A. V.; Demazeau, G.; Volkova, O. S.; Cherepanov, V. M.; Goodilin, E. A.; Knot'ko, A. V.; Isobe, M. *Phys. Rev. B* **2007**, *76*, 214407.
(42) Woodward, P. M.; Cox, D. E.; Moshopoulou, E.; Sleight, A. W.; Morimoto, S. *Phys. Rev. B* **2000**, *62*, 844.
(43) Takeda, T.; Kanno, R.; Kawamoto, Y.; Takano, M.; Kawasaki, S.; Kamiyama, T.; Izumi, F. *Solid State Sci.* **2000**, *2*, 673.

Table 2. Structural Parameters of $ACu_3V_4O_{12}$ (A = Na^+, Ca^{2+}, and Y^{3+})

	$NaCu_3V_4O_{12}$	$CaCu_3V_4O_{12}$	$YCu_3V_4O_{12}$
radius (A) (Å)	1.02	1.00	0.90
a (Å)	7.2303(3)	7.2628(6)	7.2879(1)
Cu−O (Å)	1.9371(13)	1.9526(15)	1.9614(15)
V−O (Å)	1.9114(4)	1.9189(5)	1.9251(5)
BVS(Cu)	2.24	2.15	2.10
BVS(V)	4.10	4.02	3.97

ferrimagnetic spin structure of $Cu^{2+}(S=1/2)$ and $Fe^{4+}(S=2)$ should be rewritten for preciseness as $Cu^{2+}(S=1/2,\downarrow)_3Fe^{3+}(S=5/2,\uparrow)_2Fe^{5+}(S=3/2,\uparrow)_2$, but the magnitude of the resulting magnetization is the same for both of these.

The magnetism of the low-temperature phase seems to be very different from the antiferromagnetism of $CaFeO_3$. However, if we recall that a pair of nearest-neighboring Fe atoms orient their moments only ~45° away from each other in the helicoidal spin structure of $CaFeO_3$,[44,45] these oxides may be said to be rather close to each other in fact. The presence of Cu^{2+} at the A′ site must have been a perturbation, leading to the repression of the original spin canting. The nature of the perturbation would include the aforementioned intersite charge transfer, antiferromagnetic A′−B interactions, and the changes in the Fe−O−Fe bond lengths and bond angles.

3.4. $NaCu_3V_4O_{12}$−$CaCu_3V_4O_{12}$−$YCu_3V_4O_{12}$. In contrast to the local moment behaviors in Cu^{2+} ions shown above, compounds containing V at the B site show Pauli paramagnetic and metallic behaviors and electrons of Cu ions appear to behave itinerantly. Besides, the A site in $ACu_3V_4O_{12}$ can accommodate monovalent Na, divalent Ca, and trivalent Y ions. Almost single-phase samples of $NaCu_3V_4O_{12}$, $CaCu_3V_4O_{12}$, and $YCu_3V_4O_{12}$ were synthesized under high-pressure and high-temperature conditions at 9 GPa and 1000 °C for 30 min.[46–48]

The results of structure analysis along with the A-site ionic radii[20] are summarized in Table 2. Although the A-site ionic radius decreases from Na^+ to Ca^{2+} to Y^{3+}, the lattice constant, the Cu−O distance, and the V−O distance increase from $NaCu_3V_4O_{12}$ to $CaCu_3V_4O_{12}$ to $YCu_3V_4O_{12}$. These changes in the Cu−O and V−O bond distances should result from the changes in the nominal ionic valences of Cu and V ions caused by the A cation valence changes from monovalent to divalent to trivalent. To clarify this change, we calculate the BVSs[33] of the Cu and V sites by using the obtained structural parameters, and they are also shown in Table 2. The results clearly show that both Cu and V ionic valences decrease by the "A-site doping" from Na^+ to Y^{3+}.

All of the samples show metallic behavior with low resistivity of 1−35 mΩ cm at room temperature as shown in Figure 19. Note that the resistivity shows no T^2 dependence even at low temperatures. The temperature dependence of the magnetic susceptibility measured under an external magnetic field of 1 kOe is shown in Figure 20. The data are well fitted with a simple Curie formula, $M/H = \chi_0 + C_{CW}/T$. The temperature-independent terms χ_0 for these samples are rather large, about 1.0×10^3 emu/mol, suggesting their Pauli paramagnetic nature. This implies delocalization of the electrons of both Cu and V atoms, which is consistent with the metallic properties described above. The Curie constants C_{CW}, on the other hand, are small, respectively 0.049, 0.005, and 0.009 emu K/mol for $NaCu_3V_4O_{12}$, $CaCu_3V_4O_{12}$, and $YCu_3V_4O_{12}$. If we assume that these Curie terms come from $S = 1/2$ spins, the estimated number of spins is less than 0.13 per formula unit. The Curie-like upturns observed at low temperatures thus play minor roles in the magnetic properties and might originate from small amounts of impurity phases.

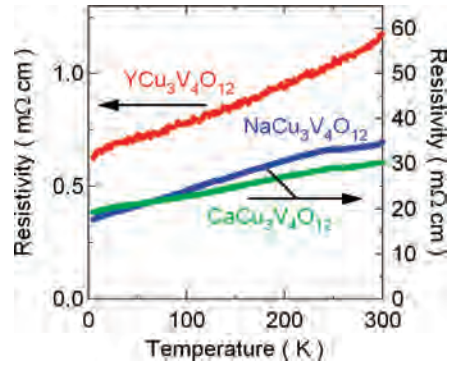

Figure 19. Temperature dependence of the resistivity of $ACu_3V_4O_{12}$ (A = Na^+, Ca^{2+}, Y^{3+}).

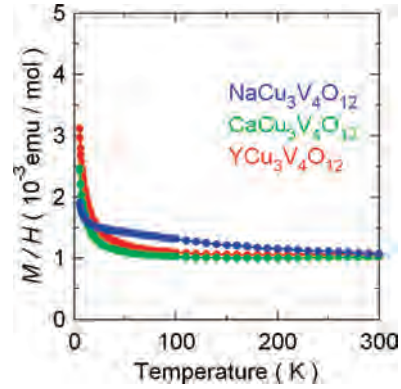

Figure 20. Temperature dependence of the magnetic susceptibility of $ACu_3V_4O_{12}$ (A = Na^+, Ca^{2+}, Y^{3+}) measured in an external magnetic field of 1 kOe.

The electronic structures of $NaCu_3V_4O_{12}$, $CaCu_3V_4O_{12}$, and $YCu_3V_4O_{12}$ were calculated by FLAPW first-principle calculations. Figure 21 shows the DOSs near E_F for the three compounds. Note that for all compounds both the Cu and V bands cross E_F, which is consistent with the metallic behavior. Changing the A-site ion from monovalent Na to divalent Ca to trivalent Y shifts E_F to a higher energy. For $NaCu_3V_4O_{12}$, $CaCu_3V_4O_{12}$, and $YCu_3V_4O_{12}$ the calculated numbers of electrons within the muffin tin spheres are respectively 27.081, 27.088, and 27.095 (corresponding valences are +1.919, +1.912, and +1.905) for the Cu site and 20.292, 20.306, and 20.325 (+2.708, +2.694, and +2.675) for the V site. The results clearly indicate that electrons are doped into both Cu and V bands within a rigid band picture by changing the A-site ion from Na^+ to Y^{3+}.

(44) Kawasaki, S.; Takano, M.; Kanno, R.; Takeda, T.; Fujimori, A. *J. Phys. Soc. Jpn.* **1998**, *67*, 1529.
(45) Mostovoy, M. *Phys. Rev. Lett.* **2005**, *94*, 137205.
(46) Kadyrova, N. I.; Zakharova, G. S.; Zainulin, Y. G.; Volkov, V. L.; Dyachkova, T. V.; Tyutyunnik, A. P.; Zubkov, V. G. *Dokl. Chem.* **2003**, *392*, 251.
(47) Katdyrova, N. I.; Tyutyunnik, A. P.; Zubkov, V. G.; Zakharova, G. S.; Volkov, V. L.; Dyachkova, T. V.; Zainulin, Y. G.; Russian, J. *Inorg. Chem.* **2003**, *48*, 1785.
(48) Shiraki, H.; Saito, T.; Azuma, M.; Shimakawa, Y. *J. Phys. Soc. Jpn.* **2008**, *77*, 64705.
(49) Chamberland, B. L.; Danielson, P. S. *J. Solid State Chem.* **1971**, *3*, 243.
(50) Falcón, H.; Alonso, J. A.; Casais, M. T.; Martínez-Lope, M. J.; Sánchez-Benítez, J. *J. Solid State Chem.* **2004**, *177*, 3099.
(51) Subramanian, M. A.; Marshall, W. J.; Calvarese, T. G.; Sleight, A. W. *J. Phys. Chem. Solids* **2003**, *64*, 1569.
(52) Labeau, M.; Bochu, B.; Joubert, J. C.; Chenavas, J. *J. Solid State Chem.* **1980**, *33*, 257.

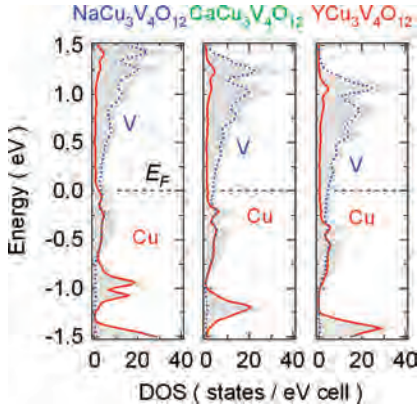

Figure 21. Calculated DOSs for $ACu_3V_4O_{12}$ (A = Na^+, Ca^{2+}, Y^{3+}). Shown are total DOSs (shaded region) and partial DOSs of Cu (solid line) and V (dashed line).

A related simple perovskite, $CaVO_3$, is also a Pauli paramagnetic metal.[45,50] The V−O distances of $CaVO_3$ and $CaCu_3V_4O_{12}$ are similar, but the tilting angles of the VO_6 octahedra differ significantly between these two compounds (the V−O−V bond angles are respectively 161.33° and 142.24° for $CaVO_3$ and $CaCu_3V_4O_{12}$). Because a large bending in the V−O−V bond angle generally causes less conduction in the hybridized orbitals of V and O atoms, the observed high conductivity in $CaCu_3V_4O_{12}$ is probably due to the involvement of Cu orbitals in conduction.

It is interesting to compare the physical properties of $ACu_3V_4O_{12}$ (A = Na^+, Ca^{2+}, and Y^{3+}) with those of other A-site-ordered perovskites such as $CaCu_3Cr_4O_{12}$ and $CaCu_3Ru_4O_{12}$, which show similar metallic conductivity.[51,52] The resistivities of $CaCu_3Cr_4O_{12}$ and $CaCu_3Ru_4O_{12}$, unlike those of $ACu_3V_4O_{12}$ (A = Na^+, Ca^{2+}, and Y^{3+}), show T^2 dependence at low temperatures as expected from a Fermi liquid picture. $CaCu_3Ru_4O_{12}$ is also reported to show heavy-fermion-like behavior with a Kondo temperature of 200 K. Enhanced temperature-independent magnetic susceptibility (χ_0 = 1.4×10^{-3} emu/Cu mol = 4.2×10^{-3} emu/mol) as well as a large electron-specific heat coefficient (γ = 28 mJ/Cu mol K^2 = 84 mJ/mol K^2) were observed and the coefficient of the T^2 resistivity satisfied the Kadowaki−Woods relation.[12] χ_0 of the present $CaCu_3V_4O_{12}$ is about 1.0×10^{-3} emu/mol, and γ obtained from the specific heat measurement is about 30 mJ/mol K^2. These values are rather large for conducting oxides but are still one third of the corresponding values for $CaCu_3Ru_4O_{12}$. Also, the most important difference between $CaCu_3Ru_4O_{12}$ and $CaCu_3V_4O_{12}$ is that the magnetic susceptibility of $CaCu_3V_4O_{12}$ does not show a characteristic maximum between 5 and 300 K. We therefore see no conclusive evidence for the heavy-fermion-like behavior in the measured temperature range in our $ACu_3V_4O_{12}$.

4. Summary

The special-ordered arrangement of the A-site ions in the perovskite structure produces $AA'_3B_4O_{12}$ complex perovskites. Jahn−Teller-distorted Cu^{2+} ions occupy the originally 12-fold-coordinated A′ site and form square-coordinated units that align perpendicularly to each other. The presence of Cu^{2+} transition-metal ions and A′−B interactions play a crucial role for the diverse and intriguing physical properties of this characteristic structure compounds.

With the B-site nonmagnetic ions, only Cu^{2+} ($S = {}^1/_2$) spins at the A′ site contribute to the magnetic properties. Direct-exchange interaction gives rise to the ferromagnetic behavior in $CaCu_3Ge_4O_{12}$ and $CaCu_3Sn_4O_{12}$, whereas involvement of Ti 3d orbitals produces the antiferromagnetic superexchange interaction in $CaCu_3Ti_4O_{12}$. When the composition of the solid solution is changed, the effective magnetic interaction between Cu^{2+} spins changes gradually from ferromagnetic to antiferromagnetic to ferromagnetic, and at critical compositions, these competing interactions are perfectly balanced to give a Weiss temperature of 0 K.

In $CaCu_3Mn_4O_{12}$, $LaCu_3Mn_4O_{12}$, and $BiCu_3Mn_4O_{12}$, B-site magnetic spins couple with the A′-site Cu spins antiferromagnetically, leading to the ferrimagnetic behaviors. Replacement of divalent Ca ions by trivalent La or Bi produces a half-metallic nature with spin-polarized conduction carriers. The large MR observed under a low magnetic field is attributed to a spin-polarized tunneling or spin-dependent scattering effect at grain boundaries.

$CaCu_3Fe_4O_{12}$ is another ferrimagnetic A-site-ordered perovskite that contains unusual high-valence Fe^{4+} ions. At 210 K, it shows charge disproportionation from Fe^{4+} to Fe^{3+} and Fe^{5+}, accompanied by an electric, magnetic, and structural change.

In the V-containing materials, localized magnetic moments of Cu completely disappear and the electrons of both the Cu and V sites behave itinerantly showing Pauli paramagnetic and metallic behaviors.

The A-site-ordered perovskites show diverse and intriguing physical properties. The combination of A and B cations open up possibilities for making compounds with new properties, which will be useful for functions in future electronics and spintronics.

Acknowledgment. The works reviewed here were done in collaboration with H. Shiraki, K. Takata, I. Yamada, T. Saito, M. Azuma, and M. Takano in ICR, Kyoto University. The author thanks T. Yamada (Tohoku University), M. Tsujimoto, H. Kurata, S. Isoda, N. Hayashi, S. Muranaka (Kyoto University), S. Shinohara, S. Mori (Osaka Prefecture University), and I. Terasaki (Waseda University) for fruitful discussions. The synchrotron radiation experiments were performed at SPring-8 with the approval of the Japan Synchrotron Radiation Research Institute. This work was partly supported by Grants-in-Aid for Scientific Research (Grants 19GS0207, 18350097, 17105002, 19014010, and 19340098), by the Joint Project of Chemical Synthesis Core Research Institutions, and by 21COE on the Kyoto Alliance for Chemistry from the Ministry of Education, Culture, Sports, Science and Technology of Japan.

IC800696U